Experimentally based model of a complex between a snake toxin and the α7 nicotinic receptor

Carole Fruchart-Gaillard*, Bernard Gilquin*, Stéphanie Antil-Delbeke*, Nicolas Le Novère†, Toru Tamiya*‡, Pierre-Jean Corringer†, Jean-Pierre Changeux†, André Ménez*§, and Denis Servent*§

*Commissariat à l'Energie Atomique, Département d'Ingénierie et d'Études des Protéines, 91191 Gif-sur-Yvette Cedex, France; †Récepteurs et Cognition, Centre National de la Recherche Scientifique/Unité de Recherche Associée D1284, Institut Pasteur, 75724 Paris Cedex, France; and ‡Department of Chemistry, Sophia University, 102-8554 Tokyo, Japan

Contributed by Jean-Pierre Changeux, December 26, 2001

To understand how snake neurotoxins interact with nicotinic acetylcholine receptors, we have elaborated an experimentally based model of the α–cobratoxin–α7 receptor complex. This model was achieved by using (*i*) a three-dimensional model of the α7 extracellular domain derived from the crystallographic structure of the homologous acetylcholine-binding protein, (*ii*) the previously solved x-ray structure of the toxin, and (*iii*) nine pairs of residues identified by cycle-mutant experiments to make contacts between the α-cobratoxin and α7 receptor. Because the receptor loop F occludes entrance of the toxin binding pocket, we submitted this loop to a dynamics simulation and selected a conformation that allowed the toxin to reach its binding site. The three-dimensional structure of the toxin–receptor complex model was validated *a posteriori* by an additional double-mutant experiment. The model shows that the toxin interacts perpendicularly to the receptor axis, in an equatorial position of the extracellular domain. The tip of the toxin central loop plugs into the receptor between two subunits, just below the functional receptor loop C, the C-terminal tail of the toxin making adjacent additional interactions at the receptor surface. The receptor establishes major contacts with the toxin by its loop C, which is assisted by principal (loops A and B) and complementary (loops D, F, and 1) functional regions. This model explains the antagonistic properties of the toxin toward the neuronal receptor and opens the way to the design of new antagonists.

The α-neurotoxins from snake venom are potent antagonists that block nicotinic acetylcholine receptors (AChRs) and hence affect synaptic transmission (1–3). Despite many studies (reviewed in ref. 4), the molecular process associated with this efficient blockage remains unclear. To approach this question, we previously studied α-cobratoxin (α-Cbtx), an α/K neurotoxin that binds to both muscular and homopentameric neuronal receptors (α7 and α8) with high affinities (4). This toxin, similar to other snake neurotoxins, is folded into three adjacent loops rich in β-sheet that emerge from a small globular core in which four disulfide bonds are located (5). By mutational analyses, the residues by which α-Cbtx interacts with the muscular-type or neuronal α7 receptors were identified previously (6, 7). The present study shows how functional residues account for the antagonistic properties of the toxin toward the α7 neuronal receptor. The α7 AChR possesses five identical α7 subunits (8) that offer five ligand-binding sites located at the interface of two subunits (9). These sites include residues located on the different functional loops described previously on the principal α7 (+) face, loops A, B, and C and on the complementary α7 (−) face, loops D, E, and F (refs. 10–13; see Fig. 1). Until now, the residues of the α7 receptor involved in snake toxin binding have remained unknown.

The aim of the present paper is fourfold. First, by an extensive mutational study we have identified α7 receptor residues involved in the interaction with α-Cbtx. Second, by using a double-mutant cycle approach we have disclosed several pairs of interacting residues in the toxin–receptor complex. Third, by

using the three-dimensional (3D) structure of an AChBP that is similar functionally and structurally to the N-terminal domain of an AChR α-subunit (14), we used a 3D model for the α7 subunit extracellular region obtained by comparative modeling [see accompanying paper on page 3210 (15)]. Fourth, by using this model, a molecular dynamics simulation of the loop F region, and the constraints derived from our pairwise analysis, we propose an experimentally based 3D model of the complex between the α-Cbtx and α7 receptor, which explains the antagonistic properties of the snake toxin toward the neuronal receptor.

Materials and Methods

Expression, Purification, and Characterization of Recombinant α-Cbtx. Recombinant wild-type and mutated α-Cbtx were obtained as described (6). Each mutant was characterized by (*i*) SDS/PAGE electrophoresis, (*ii*) analytical reverse-phase HPLC, (*iii*) electrospray mass spectroscopy, and (*iv*) circular dichroic analysis.

Expression of Wild-Type and Mutated α7 Receptor in HEK 293 Cells. A chimeric cDNA of a neuronal type nicotinic receptor (α7–5HT$_3$) was transfected into HEK 293 cells by calcium precipitation as described (11, 16). Two days after the transfection, the cells were harvested in PBS with 5 mM EDTA, washed two times with PBS, and finally resuspended in 3 ml per plate of this buffer for the binding experiments. All mutations were introduced by using the QuickChange kit (Stratagene), and the sequence was checked by automatic sequencing.

Binding Assays. Toxin affinities were determined by competition experiments on the initial rate of ^{125}I-bungarotoxin (Bgtx) binding as described (7). For receptor mutants characterized by a significant affinity decrease (Y187F, Y194R, and F186E), association kinetics of ^{125}I-Bgtx were determined to check the linearity of the association rate of the tracer during the 6-min time of the assay. The protection constants (K_p) derived from competition data correspond to the dissociation constants (11). All interacting pairs were identified by mutant-cycle experiments made at least in triplicate. We evaluated the energy of interaction between pairs of residues in the receptor and the toxin by calculating the coupling factors (Ω) and the change in coupling energy ($\Delta\Delta G_{int}$) subsequent to mutations (17, 18).

Docking of α-Cbtx on the α7 Receptor. A model of the α7 receptor derived from the x-ray structure of the AChBP (14) using MODELLER was used (see ref. 15). The x-ray structure in the

---

Abbreviations: AChR, nicotinic acetylcholine receptor; AChBP, acetylcholine-binding protein; 3D, three-dimensional; α-Cbtx, α-cobratoxin; Bgtx, bungarotoxin; α-ImI, cono-toxin ImI.

§To whom reprint requests may be addressed. E-mail: denis.servent@cea.fr or andre.menez@cea.fr.

Loops α

	loopA		loop B		loop C	
	90	98	146	152	184	196
AChBP	AAYNAISKP		GSWIHHS		SVTYSCCPE-AYED	
alpha7	LLYNSADER		GSWTYGG		ESFYECCKE-PYPD	
alpha1	VLYNNADGD		GTWTYDG		WVFYSCCPTTPYLD	

Loops non-α

	loop D		loop E		loop F	
	54	60	110	119	163	167
AChBP	WQQTTWS		VSDGEVLYMP		DDSEY	
alpha7	WLQMYWT		NSSGHCQYLP		DISGY	
gamma	WIEMQWC		SPDGCIYWLP		DPEAF	
delta	WIDHAWV		YDSGYVTWLP		DPEGF	

Fig. 1. Sequence alignment of the functional loops of α1, γ, δ, α7 and acetylcholine-binding protein (AChBP), and residues involved in toxin binding. Using α7 numbering, the sequences of the α1, γ, and δ subunits are from mouse muscular receptor, and the sequence of α7 is from chicken. Residues in green interact with a short toxin (NmmI; refs. 33, 34, 46, and 47). Those in pink interact with long toxins (α-Bgtx and α-Cbtx; refs. 7, 35, 37, and 48). The residues in blue and red interact with conotoxins GI or ImI, respectively (13, 48–50).

region 151–170 (loop F region) having a relatively low resolution (14), we explored several local positions by molecular dynamics simulation and selected the conformation providing an accessible site for the toxin. This receptor conformation differed from the original x-ray structure of AChBP by an overall rms deviation of 1.9 Å along the backbone and equal to 1.7 Å without the loop F segment. The structure of the complex was built by using all distance constraints derived by the pairwise experiments. The toxin initially was placed manually, with the side chain of R33 being located into the site defined by the Hepes in the AChBP x-ray structure. To sample all possible conformations of the toxin–receptor complex, a rigid-body high-temperature molecular dynamics simulation with reduced Van der Waals radius (0.8) was performed. Ten structures were obtained and refined by minimization through a decrease of harmonic restraints from 1,000 to 0 kcal/mol/Å^2. All the resulting structures were highly similar and varied only by a slight difference in their toxin orientations toward the receptor. The best one in terms of energy was selected. The solvent was considered implicitly using a distance-dependent dielectric constant. All calculations were carried out by using X-PLOR (19), with the force field derived from CHARMM19 (files topallh19.pro and parallh19.pro in X-PLOR 3.1). The structure of the complex was analyzed by calculation of the Van der Waals interaction energy between (*i*) each residue of the toxin with the receptor and (*ii*) each residue of the toxin versus each residue of the receptor. A contact was considered when the energy was higher than 1 kcal/mol.

Results

α7 Neuronal Receptor Residues Targeted by α-Cbtx. Six distinct segments in the α7 neuronal receptor are part of its small ligand-binding sites (reviewed in refs. 20 and 21). The principal and complementary binding sites are composed by loops A, B, and C and D, E, and F, respectively (Fig. 1). Y187 and P193 from loop C are implicated in toxin binding (7). We now have mutated 21 additional receptor residues spread on all these loops and introduced 40 mutations including alanine replacements, aromatic substitutions, or charge reversals (Table 1).

Thirteen positions, mainly located in the receptor loops A, B, and E, were mutation-insensitive, showing no significant affinity

Table 1. Binding parameters for wild type and mutants of the α-Cbtx and the α7 receptor

	Loop	K_d, nM	$K_{d(mut)}/K_{d(wt)}$	$\Delta\Delta G$, kcal/mol
α-Cbtx mutants				
WT	—	9 ± 3	1	—
D27R	II	450 ± 85	50	2.28
F29A	II	667 ± 128	74	2.51
K35A	II	99 ± 6	11	1.40
K35E	II	1298 ± 427	144	2.89
R33E	II	3055 ± 180	339	3.40
R36A	II	145 ± 15	16	1.61
R36E	II	4108 ± 506	456	3.57
F65A	Cter	139 ± 25	15.5	1.60
α7 mutants				
WT	—	9 ± 3	1.0	—
W54A	D	52 ± 8	5.8	1.02
W54F	D	43 ± 19	4.8	0.91
W54R	D	66 ± 12	7.3	**1.16**
Y58A	D	9 ± 1	1.0	0.00
D61K	D	NE	—	—
D88K	A	7 ± 1	0.8	−0.14
Y92A	A	NE	—	—
Y92R	A	46 ± 11	5.1	0.95
Y92F	A	10 ± 4	1.0	0.06
D96K	A	14 ± 5	1.5	0.26
N110S	E	42 ± 21	4.7	0.90
Q116Y	E	NE	—	—
L118A	E	18 ± 5	2.0	0.40
L118R	E	27 ± 4	3.0	0.64
W148A	B	28 ± 9	3.1	0.66
W148T	B	29 ± 3	3.2	0.68
W148F	B	17 ± 3	2.0	0.37
Y150F	B	28 ± 1	3.1	0.66
D163A	F	19 ± 2	2.0	0.43
D163K	F	54 ± 14	6.0	**1.04**
I164P	F	24 ± 15	2.7	0.57
S165E	F	36 ± 17	4.0	0.81
S165K	F	63 ± 5	7.0	**1.13**
S185V	C	12 ± 1	1.3	0.17
S185E	C	68 ± 21	7.8	**1.18**
S185K	C	9 ± 1	1.0	0.00
F186T	C	10 ± 3	1.0	0.06
F186A	C	38 ± 8	4.2	0.84
F186E	C	872 ± 100	97.0	**2.66**
Y187A	C	NE	—	—
Y187F	C	185 ± 17	21.0	**1.76**
Y187H	C	1807 ± 343	201.0	**3.15**
Y187W	C	61 ± 20	6.8	1.11
E192K	C	12 ± 1	1.3	0.17
P193A	C	19 ± 5	2.0	0.43
Y194A	C	78 ± 13	8.7	**1.26**
Y194F	C	28 ± 12	3.1	0.66
Y194R	C	269 ± 58	29.9	**1.98**
D196K	C	84 ± 5	9.3	**1.30**

Dissociation constants were determined from at least two competition experiments as described in *Materials and Methods*. The free energy of binding: $\Delta\Delta G = RT \operatorname{Ln} K_{d(mut)}/K_{d(wt)}$. NE, not expressed; WT, wild type.

decrease ($K_{d(mut)}/K_{d(wt)} < 6$; $\Delta\Delta G < 1$ kcal/mol; Table 1). By contrast, mutations introduced at eight other positions decreased the affinity in the following order: Y187 > F186 > Y194 > D196 > S185 ≥ W54, D163, and S165 (Table 1). Y187H showed the greatest effect, a 200-fold decrease in affinity ($\Delta\Delta G = 3.2$ kcal/mol), at the lower end of the scale, whereas the

NEUROBIOLOGY

mutants W54R, D163K, and S165K show just a 7-fold affinity decrease ($\Delta\Delta G = 1.1$ kcal/mol). These results suggest a predominant binding role of the receptor loop C and a less critical role for loops D and F.

Selection of Functional Residues of α-Cbtx for Pairwise Study with the Neuronal α7 Receptor. We previously identified the residues by which α-Cbtx interacts with high affinity on the neuronal α7 receptor (7). These residues belong to both the tip of the central loop (D27, F29, R33, K35, C26, C30, and R36) and the C-terminal region (F65) of the toxin. Mutants modified at four positions located on the concave face (R33 and R36), the convex face (K35), and C-terminal tail (F65) were selected for pairwise experiments. The final yield of recovery of the selected toxin mutants (R33E, K35A, K35E, R36A, R36E, and F65A) was close to 1.5 mg/liter of culture, which was sufficient for testing affinity decreases between 11- and 450-fold (Table 1).

Double-Mutant Cycle Analysis. The difference in binding energy caused by a mutation was calculated through $\Delta\Delta G = \Delta\Delta G_{wt} - \Delta\Delta G_{mut} = RT \ln [K_{d(mut)}/K_{d(wt)}]$, with $R = 1.99$ cal/mol/K and $T = 293$ K. When $\Delta\Delta G$ associated to two mutations was different from the sum of the $\Delta\Delta G$ values of each of the two single mutations, the two mutated residues were considered to be close to each other and perhaps interacting (17, 18). The coupling energy ($\Delta\Delta G_{int}$) reflecting the interaction energy for the two mutated residues was calculated from $\Delta\Delta G_{int} = RT \ln (\Omega)$, where $\Omega = K_{d(wt,wt)} \cdot K_{d(mut,mut)}/K_{d(wt,mut)} \cdot K_{d(mut,wt)}$.

Fig. 2A shows typical pairwise experiments for the four possible combinations of the mutant pair R36E and D196K. The R36E toxin mutation reduced the affinity for the wild-type receptor by 460-fold, whereas the receptor mutation D196K caused a 10-fold affinity decrease for the wild-type toxin. Together, the two mutations caused an affinity decrease of 410-fold, which does not correspond to an additive effect of the two individual mutations (4,600-fold affinity decrease). The two mutated residues are at least in proximity and perhaps in interaction. A pure additive effect is seen in Fig. 2B, in which the double mutant F65A/Y187F is characterized by a 335-fold affinity decrease, whereas the two single mutations F65A and Y187F caused affinity decreases of 15- and 21-fold, respectively. F65 and Y187 are unlikely to be in interaction.

A $\Delta\Delta G_{int}$ higher than 0.7 kcal/mol was considered as the minimum threshold for two mutated residues to be in proximity. This value, selected from other pairwise experiments (22), is 2-fold higher than the minimal threshold value characterizing interacting residues separated by 4–7 Å (18).

Table 3, which is published as supporting information on the PNAS web site, www.pnas.org, and the histogram in Fig 3 show $\Delta\Delta G_{int}$ values derived from our pairwise experiments. The data suggest that nine couplings occurred between the toxin and receptor residues. Thus, R33 seems to interact with residues W148, Y187, P193, and Y194 on the receptor. The results also show that K35 is likely to interact with D163 and F186, and R36 with D196. R36 also may be coupled to Y187, but the affinity decrease associated with R36E/Y187F was too high to allow us to make a definite conclusion. Finally, toxin F65 may interact with receptors F186 and P193, suggesting that the toxin C-terminal tail is in proximity to the receptor loop C.

Docking of α-Cbtx on a Model of α7 Receptor. Recently, the crystal structure of an AChBP functional and structural analog to the N-terminal domain of an AChR α-subunit was determined (14). It displays 24% sequence identity with the extracellular region of the α7 receptor. This value increases from 40 to 60% in functional loop regions (Fig. 1). A structural model of the α7
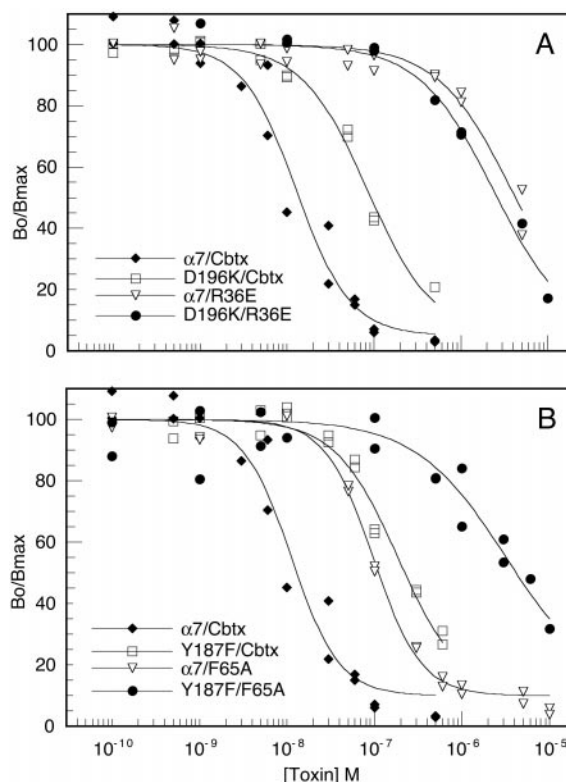

Fig. 2. Inhibition of the initial rate of ^{125}I-Bgtx binding to wild-type and mutated α7 receptors by wild-type and mutant α-Cbtx. (*A*) Binding competition experiments with the wild-type and R36E α-Cbtx toward the wild-type and D196K receptor mutant expressed in transfected HEK 293 cells. (*B*) Shown is as described for *A* for the mutant pair α7 Y187F–α-Cbtx F65A.

receptor was elaborated by using MODELLER with the x-ray structure of AChBP as template, and the resulting model was characterized by an rms deviation of 0.71 Å as compared with the original structure (see ref. 15). We performed a molecular dynamics simulation of the region 151–170, the resolution of
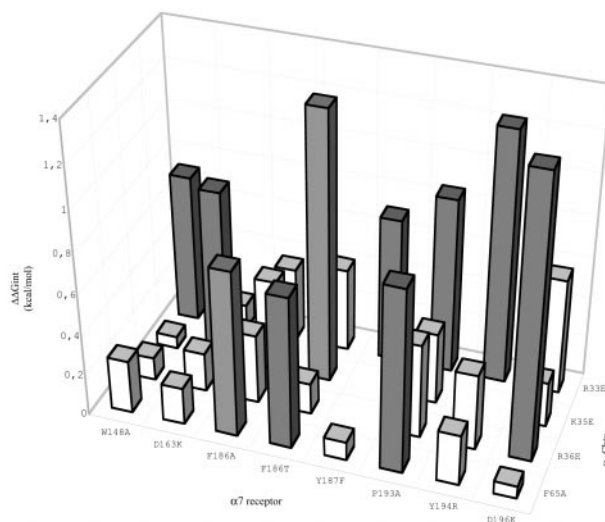

Fig. 3. Variation in free energy of interaction ($\Delta\Delta G_{int}$) associated with the binding of α-Cbtx mutant on mutated α7 receptors. The *x*, *y*, and *z* axes represent the α7 receptor mutants, the absolute values of $\Delta\Delta G_{int}$, and the toxin mutants, respectively.
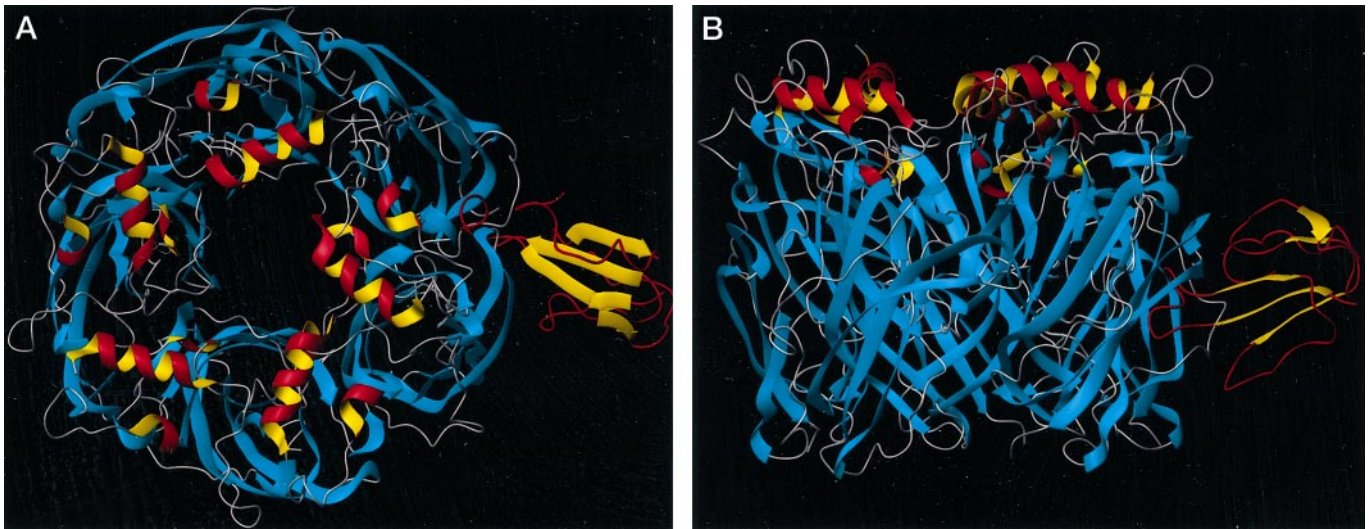
Fruchart-Gaillard *et al.*

Fig. 4. Structural model of the α7 receptor–α-Cbtx complex. The five subunits of the receptor are depicted with their β-sheets colored blue and the apical helices colored red and yellow. One toxin molecule is shown at an arbitrary subunit interface with its β-sheet in yellow and its backbone in red. (*A*) Top view of the model. (*B*) The receptor is seen perpendicularly to the 5-fold axis with the toxin in an equatorial position.

which is low in the x-ray structure (14), and hence we selected a conformation allowing the toxin to reach its binding site.

A model of the 3D structure of the receptor–toxin complex was calculated by using distances derived from our pairwise experiments. The resulting complex has low internal energy with only one violation (0.8 Å). Calculation of the Van der Waals interaction energies revealed that 13 residues of the toxin were in contact with the receptor, nine of which were identified previously by mutagenesis experiments (7). These residues include the critical R33, F29, and R36. The others have not been tested (R68 and K69) or were insensitive to mutation (S31 and I32; ref. 7). Inspection of the structure of the complex showed that the average distances between side chain atoms of interacting residues globally agree with the energy values deduced from pairwise analyses. The pairs Y194/R33 and D196/R36 displayed the shortest distances (4.5–5Å) with corresponding $\Delta\Delta G_{int}$ values higher than 1.2 kcal/mol. The other interacting

pairs displayed larger distances (5–8 Å) with $\Delta\Delta G_{int}$ values ranging from 0.7 to 0.9 kcal/mol. We observed only one exception for the pair F186/K35 characterized by a high $\Delta\Delta G_{int}$ value (1.3 kcal/mol) and a large distance, close to 11 Å. Nevertheless, their backbone atoms are close together.

On the Contact Regions in the Toxin–Receptor Complex. Fig. 4*A* shows a top view of a toxin molecule bound to the pentameric model of the α7 receptor. The tip of the toxin central loop plugs into the receptor at the interface formed by two subunits. The C-terminal tail also stabilizes the complex but interacts only with residues at the receptor surface. Neither toxin loop I nor loop III interact with the receptor, which is in agreement with our mutational data (7). Although 75% of the surface of the toxin remains outside the complex, the buried surface is equal to 2,450 Å², as observed for typical protein–protein interactions (23, 24). Viewed perpendicularly to the 5-fold axis of the pentamer, the
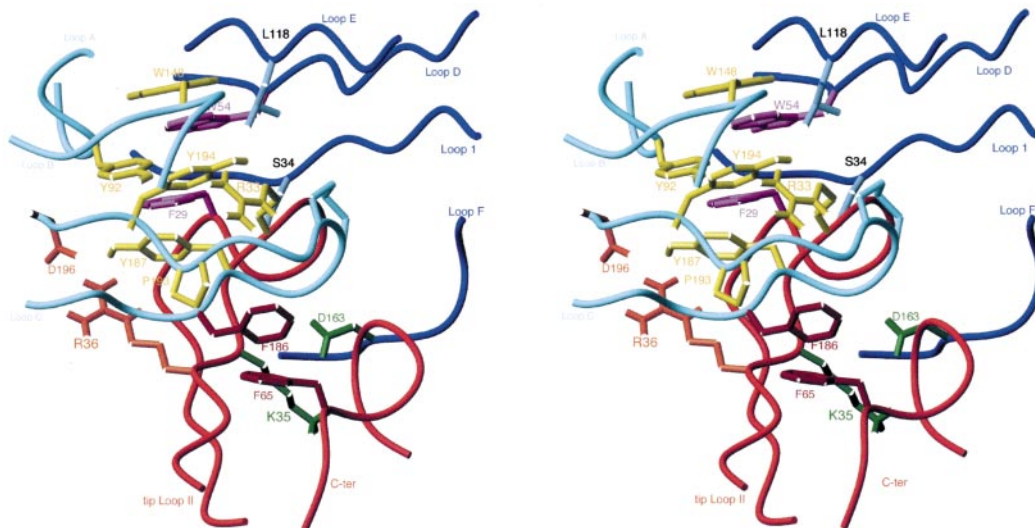

Fig. 5. Stereo representation of the toxin binding site. The backbone of the principal (A, B, and C in the α face) and complementary (D, E, F, and 1 in the non-α face) loops of the receptor are colored cyan and blue, respectively. The toxin backbone of the tip of loop II and C-terminal tail is colored red. The residues that form interacting pairs have their side chains colored similarly.

NEUROBIOLOGY

toxin lies equatorially to the extracellular domain, with its concave side facing the viewer with loops I and III orientated toward the top and bottom of the receptor domain, respectively (Fig. 4*B*). The receptor loop C is just above the tip of toxin loop II, and the toxin C-terminal tail is in proximity to intersubunit interfaces (Fig. 4*B*).

The tip of the toxin central loop makes several contacts with functional loops from the principal and complementary faces of the receptor (Fig. 5). For example, the side chain of R33 fits nicely into the cavity where the Hepes molecule is seen in the AChBP structure (14) and is located at the center of the cage delineated by the aromatic residues from loops B (W148), C (Y187 and Y194), and D (W54). The calculated Van der Waals energies (not shown) agree with our pairwise analyses, showing that all the functional α7 receptor residues belong to the standard functional loops (Fig. 5). Also, the toxin does not interact with loop E of the receptor, which is in agreement with the lack of mutation-sensitive residues in this loop. The model also suggests a number of contacts not probed by our pairwise analyses in loops A, B, C, D, and F. Thus, α7E188 from loop C interacts with five residues at the tip of the toxin loop II, and Y92 and W54 in the receptor loops A and D are closed to α-CbtxF29. Finally, S32 and S34 in the receptor make contact with S31 and I32 in the toxin loop II. This receptor region, which includes S34, was shown to interact with conotoxin PnIB (25), and the homologous residue in the muscular receptor (δS36 or γK34) binds to carbamylcholine and conotoxin MI (26, 27). This position is attributed to the complementary region loop 1 (28).

Discussion

The experimentally based model of the toxin–receptor complex presented here helps to understand how α-Cbtx from *Naja kaouthia* blocks the α7 receptor. This was done by using (*i*) a model of the α7 receptor (see ref. 15) derived from the x-ray structure of the homologous AChBP (14), (*ii*) the x-ray structure of the toxin (5), and (*iii*) nine constraints derived from the identified pairwise interactions. The 3D model of the complex reveals that the toxin's central loop plugs into the interface formed by two subunits of the receptor, whereas the toxin C-terminal tail only makes external contacts at the receptor surface. Strikingly, our receptor model did not allow the toxin to reach its binding site, the loop F region closing the possible entrance. This situation agrees with the hypothesis that the template structure of AChBP may adopt a desensitized state conformation (29), to which snake toxins would not bind. Because the loop F region is flexible in the template x-ray structure, we followed a molecular dynamics simulation and selected a conformation of this region appropriate for toxin to penetrate into the receptor. We suggest that the differential conformations thus adopted by the loop F region may constitute one of the preliminary steps of the global reorganization associated with the allosteric transition of the receptor between desensitized and resting states.

The proximity between two residues found to interact in the model but not tested in our mutational analysis was evaluated *a posteriori*. The selected interacting residues are α7W54 and α-Cbtx F29, the side chains of which are separated by 5 Å in the complex model. The toxin mutation F29A and the receptor mutation W54A caused affinity decreases of 74- and 6-fold, respectively (Table 2), indicating that both residues are important for stabilizing the complex. More importantly, the double mutation causes a nonadditive free-energy change ($\Delta\Delta G_{int}$ of −0.93 kcal/mol), indicating that these residues are in proximity, validating the modeling results.

The model presented in this paper shows that α-Cbtx binds to the α7 AChR by predominantly interacting with the loop C on the principal face, responsible for 60% of all observed Van der

Table 2. Mutant cycle analysis for the α-Cbtx F29-α7 W54 receptor mutant pair

Mutations		K_d, nM	$K_{d(mut)}/K_{d(wt)}$	Ω	$\Delta\Delta G_{int}$, kcal/mol
αCbtx	α7AChR				
WT	WT	9 ± 3	1	—	—
WT	W54A	52 ± 8	5.8	—	—
F29A	WT	667 ± 128	74	—	—
F29A	W54A	789 ± 78	88	−4.9	−0.93

Dissociation constants and $\Delta\Delta G$ are determined as described in Table 1. The calculation of the coupling factor Ω and the coupling energy $\Delta\Delta G_{int}$ is described in the text. Ω values less than 1 were inverted and indicated with a negative sign.

Waals contacts. Other functional loops also contribute to the binding but more moderately. Thus a weak binding role was found for loops A (Y92) and B (W148) on the receptor (+) face, whereas loops D (W54), F (D163), and 1 (S34) on the (−) face play a more important functional role. Only loop E (L118) seems not to interact with the toxin (Fig. 5).

How can this situation explain the antagonistic property of the snake toxin? Small ligands also bind at the interface of two α7 subunits (10–13) on loops A, B, C, D, and F for ACh, nicotine or DHβE and A, B, C, and E for conotoxin ImI (α-ImI). This and previous (13) pairwise analyses indicate that α-ImI and α-Cbtx clearly bind to overlapping sites. Even both toxins possess an arginine residue that seem to establish homologous cation π interactions with the α7 receptor. Thus, R33 in α-Cbtx interacts with Y194 in the chick α7 receptor, and R7 in α-ImI is coupled to the homologous Y195 in the rat α7 receptor (13). This finding not only agrees with the observation that the helical-type scaffold of α-ImI superimposes with the tip of the central loop of α-Cbtx (30) but also that two structurally unrelated toxins may establish highly homologous binding functions (31). Therefore, despite its rather large size the snake toxin "behaves like a small ligand," with the very tip of its central loop that can plug similarly into the cavity offered by the receptor interface. This situation explains the antagonistic properties of snake toxins toward the α7 AChR.

During the completion of this work, a proposal for the 3D structure of a complex between a snake toxin and AChBP had been reported (32). These authors based their proposition on an observed structural analogy between the AChBP loop C and a mimotope peptide bound to a snake toxin. The overall relative locations of the toxin and the receptor loop C were globally similar in both studies. However, the manner by which the toxin interacted with the receptor complementary face differed substantially in both studies. In particular, structural clashes appeared in the AChBP–α-Bgtx complex model (32) between the toxin and the receptor loops D, F, and 1, excluding the possibility that the toxin recognizes the receptor (AChBP) in this conformation.

How do the binding modes of snake toxins to α7 and muscular receptors compare with each other? Clearly the loop C that contains highly functional residues conserved in both receptors plays a predominant binding role. The evidence that supports that conclusion includes (*i*) mutational analyses with short chain (33, 34) and long chain (35–37) toxins, (*ii*) the use of synthetic receptor peptides of the region 180–200 (38, 39), (*iii*) studies on the resistance of various species to toxins (40, 41), (*iv*) direct affinity labeling experiments (42), and (*v*) resolution of solution structures of the complexes formed between α-Bgtx and peptides (32, 43–45). Also, the additional binding function observed here for other α and non-α loops was postulated for muscular receptors (46–48). However, the homopentameric α7 receptor and heteropentameric muscular subtypes also display marked

differences with respect to toxin binding. Thus five toxins, in principle, can interact identically on the $\alpha7$ receptor, whereas the muscular AChR displays only two toxin binding sites. Also, the toxin may interact with different orientations at the two subunit interfaces of the muscular subtype (46). Therefore, although snake toxins may bind in a globally similar manner on neuronal $\alpha7$ and muscular receptors especially through their loop C, a

number of local deviations in toxins and/or receptors are required for highly specific and potent toxin-receptor recognition to occur.

1. Chang, C. C. & Lee, C. Y. (1963) *Arch. Int. Pharmacodyn. Ther.* **144,** 241–257.
2. Changeux, J. P., Kasai, M. & Lee, C. Y. (1970) *Proc. Natl. Acad. Sci. USA* **67,** 1241–1247.
3. Endo, T. & Tamiya, N. (1991) in *Snake Toxins*, ed. Harvey, A. L. (Pergamon, New York), pp. 165–222.
4. Servent, D. & Ménez, A. (2001) in *Handbook of Neurotoxicology*, ed. Massaro, E. J. (Humana, Totowa, NJ), Vol. 1, pp. 385–425.
5. Betzel, C., Lange, G., Pal, G. P., Wilson, K. S., Maelicke, A. & Saenger, W. (1991) *J. Biol. Chem.* **266,** 21530–21536.
6. Antil, S., Servent, D. & Ménez, A. (1999) *J. Biol. Chem.* **274,** 34851–34858.
7. Antil-Delbeke, S., Gaillard, C., Tamiya, T., Corringer, P. J., Changeux, J. P., Servent, D. & Ménez, A. (2000) *J. Biol. Chem.* **275,** 29594–29601.
8. Couturier, S., Bertrand, D., Matter, J. M., Hernandez, M. C., Bertrand, S., Millar, N., Valera, S., Barkas, T. & Ballivet, M. (1990) *Neuron* **5,** 847–856.
9. Palma, E., Bertrand, S., Binzoni, T. & Bertrand, D. (1996) *J. Physiol.* **491,** 151–161.
10. Galzi, J. L., Bertrand, D., Devillers-Thiéry, A., Revah, F., Bertrand, S. & Changeux, J. P. (1991) *FEBS Lett.* **294,** 198–202.
11. Corringer, P. J., Galzi, J. L., Eiselé, J. L., Bertrand, S., Changeux, J. P. & Bertrand, D. (1995) *J. Biol. Chem.* **270,** 11749–11752.
12. Corringer, P. J., Bertrand, S., Bohler, S., Edelstein, S. J., Changeux, J. P. & Bertrand, D. (1998) *J. Neurosci.* **18,** 648–657.
13. Quiram, P. A., Jones, J. J. & Sine, S. M. (1999) *J. Biol. Chem.* **274,** 19517–19524.
14. Brejc, K., van Dijk, W. J., Klaassen, R. M., Schuurmans, M., van der Oost, J., Smit, A. B. & Sixma, T. K. (2001) *Nature (London)* **411,** 269–276.
15. Le Novère, N., Grutter, T. & Changeux, J.-P. (2002) *Proc. Natl. Acad. Sci. USA* **99,** 3210–3215.
16. Servent, D., Winckler-Dietrich, V., Hu, H. Y., Kessler, P., Drevet, P., Bertrand, D. & Ménez, A. (1997) *J. Biol. Chem.* **272,** 24279–24286.
17. Hidalgo, P. & MacKinnon, R. (1995) *Science* **268,** 307–310.
18. Schreiber, G. & Fersht, A. R. (1995) *J. Mol. Biol.* **248,** 478–486.
19. Brünger, A. Y. (1992) X-PLOR, A System for X-ray Crystallography and NMR (Yale Univ. Press, New Haven, CT), Version 3.1.
20. Le Novère, N., Corringer, P. J. & Changeux, J. P. (1999) *Biophys. J.* **76,** 2329–2345.
21. Corringer, P. J., Le Novère, N. & Changeux, J. P. (2000) *Annu. Rev. Pharmacol. Toxicol.* **40,** 431–458.
22. Rauer, H., Lanigan, M. D., Pennington, M. W., Aiyar, J., Ghanshani, S., Cahalan, M. D., Norton, R. S. & Chandy, K. G. (2000) *J. Biol. Chem.* **275,** 1201–1208.
23. Lo Conte, L., Chothia, C. & Janin, J. (1999) *J. Mol. Biol.* **285,** 2177–2198.
24. Janin, J. & Chothia, C. (1990) *J. Biol. Chem.* **265,** 16027–16030.
25. Quiram, P. A., McIntosh, J. M. & Sine, S. M. (2000) *J. Biol. Chem.* **275,** 4889–4896.
26. Prince, R. J. & Sine, S. M. (1996) *J. Biol. Chem.* **271,** 25770–25777.
27. Bren, M. & Sine, S. M. (2000) *J. Biol. Chem.* **275,** 12692–12700.
28. Tsigelny, I., Sugiyama, N., Sine, S. M. & Taylor, P. (1997) *Biophys. J.* **73,** 52–66.
29. Grutter, T. & Changeux, J. P. (2001) *Trends Biochem. Sci.* **26,** 459–463.
30. Maslennikov, I. V., Shenkarev, Z. O., Zhmak, M. N., Ivanov, V. T., Methfessel, C., Tsetlin, V. I. & Arseniev, A. S. (1999) *FEBS Lett.* **444,** 275–280.
31. Ménez, A. (1998) *Toxicon* **36,** 1557–1572.
32. Harel, M., Kasher, R., Nicolas, A., Guss, J. M., Balass, M., Fridkin, M., Smit, A. B., Brejc, K., Sixma, T. K., Katchalski-Katzir, E., Sussman, J. L. & Fuchs, S. (2001) *Neuron* **32,** 265–275.
33. Ackermann, E. J., Ang, E. T. H., Kanter, J. R., Tsigelny, I. & Taylor, P. (1998) *J. Biol. Chem.* **273,** 10958–10964.
34. Malany, S., Osaka, H., Sine, S. M. & Taylor, P. (2000) *Biochemistry* **39,** 15388–15398.
35. Spura, A., Russin, T. S., Freedman, N. D., Grant, M., McLaughlin, J. Y. & Hawrot, E. (1999) *Biochemistry* **38,** 4912–4921.
36. Spura, A., Riel, R. U., Freedman, N. D., Agraval, S., Seto, S. & Hawrot, E. (2000) *J. Biol. Chem.* **275,** 22452–22460.
37. Levandoski, M. M., Lin, Y. X., Moise, L., McLaughlin, J. T., Cooper, E. & Hawrot, E. (1999) *J. Biol. Chem.* **274,** 26113–26119.
38. Lentz, T. L. (1995) *Biochemistry* **34,** 1316–1322.
39. McLane, K. E., Dunn, S. J. M., Manfredi, A. A., Conti-Tronconi, B. M. & Raftery, M. A. (1996) *Protein Eng. Des.* **10,** 289–352.
40. Keller, S. H., Kreienkamp, H. J., Kawanishi, C. & Taylor, P. (1995) *J. Biol. Chem.* **270,** 4165–4171.
41. Kreienkamp, H. J., Sine, S. M., Maeda, R. K. & Taylor, P. (1994) *J. Biol. Chem.* **269,** 8108–8114.
42. Michalet, S., Teixeira, F., Gilquin, B., Mourier, G., Servent, D., Drevet, P., Binder, P., Tzartos, S., Ménez, A. & Kessler, P. (2000) *J. Biol. Chem.* **275,** 25608–25615.
43. Samson, A. O., Chill, J. H., Rodriguez, E., Scherf, T. & Anglister, J. (2001) *Biochemistry* **40,** 5464–5473.
44. Zeng, H., Moise, L., Grant, M. A. & Hawrot, E. (2001) *J. Biol. Chem.* **276,** 22930–22940.
45. Scherf, T., Kasher, R., Balass, M., Fridkin, M., Fuchs, S. & Katchalski-Katzir, E. (2001) *Proc. Natl. Acad. Sci. USA* **98,** 6629–6634.
46. Osaka, H., Malany, S., Kanter, J. R., Sine, S. M. & Taylor, P. (1999) *J. Biol. Chem.* **274,** 9581–9586.
47. Osaka, H., Malany, S., Molles, B. E., Sine, S. M. & Taylor, P. (2000) *J. Biol. Chem.* **275,** 5478–5484.
48. Sine, S. M. (1997) *J. Biol. Chem.* **272,** 23521–23527.
49. Sugiyama, N., Marchot, P., Kawanishi, C., Osaka, H., Molles, B., Sine, S. M. & Taylor, P. (1998) *Mol. Pharmacol.* **53,** 787–794.
50. Chiara, D. C., Xie, Y. & Cohen, J. B. (1999) *Biochemistry* **38,** 6689–6698.

NEUROBIOLOGY